Fundamental Global Model for the Structures and Energetics of Nanocrystalline Ionic Solids

Elena Bichoutskaia* and Nicholas C. Pyper

University Chemical Laboratory, Lensfield Road, Cambridge CB2 1EW, U.K.

Received: October 11, 2005; In Final Form: December 23, 2005

This paper presents a general theory elucidating the relationships between the structures and cohesive energetics of alkali halide nanocrystals consisting of small sections of bulk rocksalt structures with m_1 and m_2 rows but infinite along the z axis. The theory introduces the electrostatic interactions between the ions treated as point charges and the short-range repulsions between the closest ion neighbors with the latter terms written in the Born form Ar^{-n}. Minimum energy structures are defined by the distances a_e and b_e separating the closest ions perpendicular and parallel to the z direction. The ratio a_e/b_e, defining the crystal shape, is independent of the strength A of the short-range repulsion, greater than the bulk value of unity, and increases with decrease of the crystal cross section or n. This ratio tends toward unity in the hard sphere limit of infinite n. Both $b_e/R_e^{6:6}$ and $a_e/R_e^{6:6}$, with the bulk separation $R_e^{6:6}$, are less than one, increase with increase of the crystal cross section or n, and are independent of A if this is independent of structure. The structural dependence of A increases its value with a decreasing crystal cross section rendering closer to unity the ratios a_e/b_e, $b_e/R_e^{6:6}$, and $a_e/R_e^{6:6}$. Energy gains on relaxing the crystal toward equilibrium from its bulk separations decrease with increase of the crystal cross section or n, being about 60 kJ/mol for a one-dimensional chain with $n = 6$ but 0.5 kJ/mol for $m_1 = m_2 = 4$ with $n = 12$. The energy gained on relaxing to a structure with a_e/b_e constrained at unity is about 10 times greater than the further energy gains consequent on removing this constraint. The present theory neglecting the interaction between ions and the encapsulating nanotube explains the experimentally measured $b_e/R_e^{6:6}$ ratios. The observation that the $a_e/R_e^{6:6}$ values are greater than one shows that ion−wall interactions are important in determining the values of a_e.

1. Motivation

Single walled carbon nanotubes (SWNTs) are ideal nanometric objects which facilitate the formation of low-dimensional ordered structures within their cavity. Filling materials deliberately introduced in SWNTs range from single elements, specifically, heavy metals such as Ru,[1] Bi,[2] Ag,[3] Au, Pt, and Pd[4] to molecules such as fullerenes,[5,6] metal oxides,[7] and halides.[8−13] The main interests of filling SWNTs are to enforce the encapsulated material to adopt a low-dimensional morphology and to produce templates for atomically regulated low-dimensional crystal growth.[14] Recently, the crystal growth behavior of ionic solids in SWNTs, and especially of single binary alkali halides such as KI, has been thoroughly investigated both experimentally[10−12] and theoretically.[15−17] The experimental studies revealed that the structures of the encapsulated crystals were systematically distorted from those of the bulk, while the theoretical studies, using mainly molecular dynamics simulations, yielded valuable insights into the possible mechanisms of crystal growth inside a SWNT.

In this paper, a general analytical theory for the structures and energetics of nanocrystalline ionic solids is presented. The aim is not only to present a comprehensive mathematical formulation but also to provide physical insights into the resulting predictions. The paper is concerned with structures of the alkali halides encapsulated with the ⟨001⟩ direction parallel to the nanotube axis. Although such crystals are, in principle, infinite in extent along the z direction, a view along this direction will show a small plane consisting of m_1 rows and m_2 columns
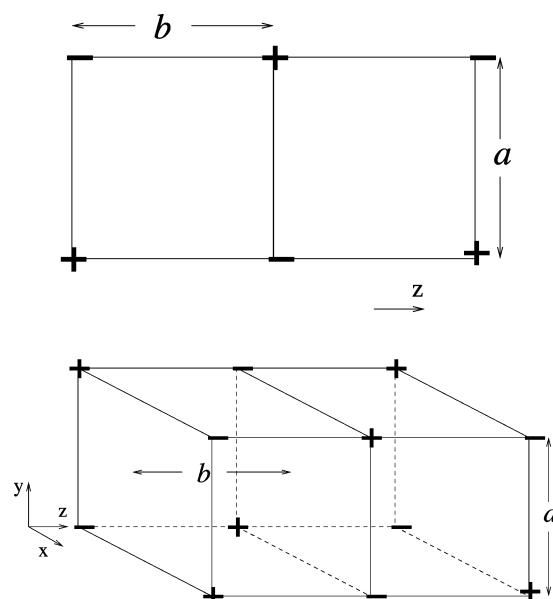
Figure 1. Structures of 2 × 1 (top) and 2 × 2 (bottom) nanocrystals, infinite along the z direction, showing one unit repeat.

of ions with alternating cations and anions in each row. The geometry of such a crystal is defined after specifying both the distance b between the successive planes encounted on increasing the z coordinate and the distance a between neighboring ions in the same plane. These coordinates are depicted in Figure 1. Understanding these structures first requires that one disentangles the effects which arise solely from the finite extent of the crystal in two of the directions from any further effects

---

* Corresponding author.

Model for Properties of Nanocrystalline Ionic Solids

J. Phys. Chem. B, Vol. 110, No. 12, 2006 **5937**

TABLE 1: Coefficients Determining the Interchain Electrostatic and Repulsion Energies

crystallite	n_c	repulsion energy	Madelung energy		
		C	$M_b(1)$	q	n_{cp}^q
2×1	2	1	0.116741	1	$n_{cp}^1 = 1$
2×2	4	2	0.204910	1, 2	$n_{cp}^1 = 4$, $n_{cp}^2 = 2$
3×3	9	$^8/_3$	0.259785	1, 2, 4, 5, 8	$n_{cp}^1 = 12$, $n_{cp}^2 = 8$, $n_{cp}^4 = 6$, $n_{cp}^5 = 8$, $n_{cp}^8 = 2$
4×4	16	3	0.289080	1, 2, 4, 5, 8, 9, 10, 13, 18	$n_{cp}^1 = 24$, $n_{cp}^2 = 18$, $n_{cp}^4 = 16$, $n_{cp}^5 = 24$, $n_{cp}^8 = 8$, $n_{cp}^9 = 8$, $n_{cp}^{10} = 12$, $n_{cp}^{13} = 8$, $n_{cp}^{18} = 2$
bulk	∞	4	0.361270		

generated from explicit interactions between the encapsulated ions and the nanotube wall. The answering of this question raises the possibility that the nanotube plays no role beyond that of an essentially passive spectator which simply constrains the crystal geometry by defining the numbers (m_1 and m_2) of rows and columns in the planes. In this event, the wall would provide no more than a potential of the square well type in which the interaction with any ion is zero unless it directly encounters the wall in which event the interaction is sufficiently large as to expel the ion from the immediate vicinity of the wall. Disentangling the effects of ion−wall interactions from those generated solely by the reduced dimensionality of the crystals requires that one understands the structures and energetics of isolated crystals of the type shown in Figure 1, which, therefore, form the main subject of the present investigation. The overarching objective of this paper is therefore to develop a general theory which explains the inter-relationships between both crystals differing only in the number (m) of rows and columns in the planes and between crystals having the same m but chemically different ions. Such a theory must also expose the relationship between the nanocrystals and the bulk material having the rock-salt structure, thereby showing how the properties of the nanocrystals evolve toward those of the bulk as the number of rows and columns in the planes is increased. The initial step in generating a physically transparent yet general theory of all such nanocrystals is to consider only the dominant interactions. These are the electrostatic interactions between the ions considered as point charges and the short-range repulsive interactions between each cation and just its immediately neighboring anions. This approach not only ensures that the theory will be mathematically tractable and appear in a relatively simple form but is also provides the benchmark against which the effects of introducing further but smaller interactions can be gauged. Such a theory should ideally incorporate the effects of chemical variation of the ions through a very small number of parameters defining the short-range interactions. The present theory can therefore be regarded as the natural extension, to nanocrystals, of the classic Born description[18] of bulk materials.

2. Analytic Deduction of Overall Structural Trends

2.1. Basic Definitions. The Born model,[18] although semiempirical, provides the simplest satisfactory overall account of the cohesion of bulk ionic crystals. This emerges as the balance between the overall Coulombic attractions of the ions, treated as point charges, and the short-range repulsive forces between the closest pairs of ions. The latter interactions, maintaining the crystal at equilibrium against the attractive point coulomb term, can, conceptually, be taken to include all effects arising from the finite spatial extension of the ions. These include not only the overlap induced repulsion that is ultimately a purely quantum effect originating from the Pauli principle but also any modifications of the purely electrostatic interactions. These two interactions, namely, the point Coulombic and the short-range repulsion, will also make the largest contributions to the cohesive

energy, which in turn determines the structure of the nanocrystals in the absence of interaction with the encapsulating nanotube. The simplest yet still mathematically tractable overall account of the structures and cohesive energetics of such crystals is therefore developed by including only these two terms. The need for avoiding excessively complicated and possibly intractable mathematics dictates that the short-range repulsion between two ions separated by a distance r is taken to have the original Born form A/r^n rather than the possibly more accurate Born−Mayer expression.[18] It is now well established[19] from measurements of the compressibilities of a wide range of essentially ionic crystals that the Born exponent n is the average of independent cation and anion contributions. The contribution from an ion having a $2p^6$ outermost electronic configuration is 7; those from ions having such configurations of $3p^6$, $4p^6$, and $5p^6$ are 9, 10, and 12, respectively, while the Li^+ contribution is 5.

For any of the nanocrystalline alkali halides, the individual planes will necessarily be square in cross section in the lowest energy structure because there is no mathematical distinction between the cations and anions in the present Born type model. The geometry is therefore defined by just the two parameters a and b defined in section 1. For a nanocrystal containing 1 mol of stoichiometric formula units and with geometry thus defined, the total crystal cohesive energy $N_A U(a, b)$, negative for a bound crystal and measured relative to the sum of the energies of the free isolated ions, is given by

$$N_A U(a, b) = N_A \left(U_{mad}(a, b) + \frac{2A}{b^n} + \frac{CA}{a^n} \right) \qquad (1)$$

Here, N_A is Avogadros number so that $N_A U_{mad}(a, b)$ is the total Madelung energy of 1 mol. The term $2A/b^n$ describes the repulsion experienced by any one ion with its two neighboring ions in the same chain. The constant C is defined such that $N_A CA/a^n$ is, for 1 mol, the sum of all the short-range repulsions between ions in neighboring chains. Numerical values of these constants are reported in Table 1. For systems, such as the 2×2 nanocrystal or a bulk cubic crystal, in which all the chains are located in the same environment, the constant C is the number of anions located at distance a from any one cation, any such anion being in a neighboring chain. Thus, for such systems, C equals the coordination number minus 2. The derivation of C for systems in which not all the chains are in the same environment can be illustrated by considering 1 mol of a 3×3 nanocrystal, this having $N_A/9$ cations in each chain. Each cation at the center of one of the planes, having also cations at the four corners, experiences repulsion from four anions, so that all such cations contribute $4N_A/9$ repulsions to the molar energy. Although each cation at the corner experiences only two such repulsions, there are four such cations, so that all these cations contribute $8N_A/9$ repulsions to the molar energy. Planes of the neighboring type contain only cations at the middle of the edges, there being four such ions. Since each of these experiences three repulsions, all such ions contribute $12N_A/9$

repulsions to the molar energy. The total number of repulsions from cations in three of the environments just considered is $24N_A/9$ which explains the value of 8/3 for C reported in Table 1. The C value for the 4×4 crystal can be similarly derived. The observation that every pair of ions experiencing such a short-range repulsion will also contribute $-1/a$ to the Madelung energy of the crystal allows the C constants to be extracted from the calculation of $U_{mad}(a, b)$ to be presented in section 2.3.

2.2. Application to a One-Dimensional Crystal. For a one-dimensional (1D) crystal consisting of a single alternating sequence of N_A cations and N_A anions, the form of expression 1 for its cohesive energy $U_{1D}(b)$, depending on just the single geometrical parameter b, reduces to

$$U_{1D}(b) = -\frac{M_{1D}}{b} + \frac{2A}{b^n} \tag{2}$$

The Madelung constant M_{1D} is readily evaluated through

$$M_{1D} = 2\sum_{m=1}^{\infty} \frac{(-1)^{m+1}}{m} = 2\ln 2 \tag{3}$$

The equilibrium separation, b_e^{1D}, is that minimizing $U_{1D}(b)$ and is found from 2 to be given by

$$b_e^{1D} = \left(\frac{2nA}{M_{1D}}\right)^{1/(n-1)} \tag{4}$$

The standard expression for the cohesive energy of 1 mol of bulk three-dimensional crystal having the rock-salt structure with internuclear separation R differs from 2 only in that M_{1D} is replaced by the Madelung constant $M_{6:6} (= 1.74756456)$ and that the repulsive term becomes $6A/R^n$. For this bulk crystal, the equilibrium separation, denoted $R_e^{6:6}$, is given by

$$R_e^{6:6} = \left(\frac{6nA}{M_{6:6}}\right)^{1/(n-1)} \tag{5}$$

It follows from 4 and 5 that the ratio of the equilibrium separations in the 1D chain and the bulk is given by

$$\frac{b_e^{1D}}{R_e^{6:6}} = \left(\frac{1}{3}\frac{M_{6:6}}{M_{1D}}\right)^{1/(n-1)} \tag{6}$$

Result 6 shows that the fractional change in the interionic distance on passing from the bulk to the 1D chain is independent of the strength, as defined by A, of the short-range repulsion. It is shown in the next section that this is a general result valid for all the nanocrystals. Thus, relation 6 shows that the fractional changes in the geometry are determined solely by the range of the repulsion defined by the exponent n. Since the ratio in brackets in 6 is less than unity, the ionic separation in the chain is predicted to be contracted relative to that of the bulk. It is predicted from the numerical values for $b_e^{1D}/R_e^{6:6}$, equal to $0.4202^{1/(n-1)}$ and depicted in Figure 2 as a function of n, that the greatest fractional contraction of 0.841 will occur for LiF, for which n is 6. It is further predicted from this relation that the contraction decreases with increasing n until it vanishes in the hard sphere limit of n tending to infinity. In physical terms, it can be seen that these contractions arise because, on passing from the bulk to the 1D system, the factor of 3 reduction in the number of short-range repulsions is much greater than the fractional reduction in the Madelung energy by the ratio $(2 \ln 2)/1.747$.
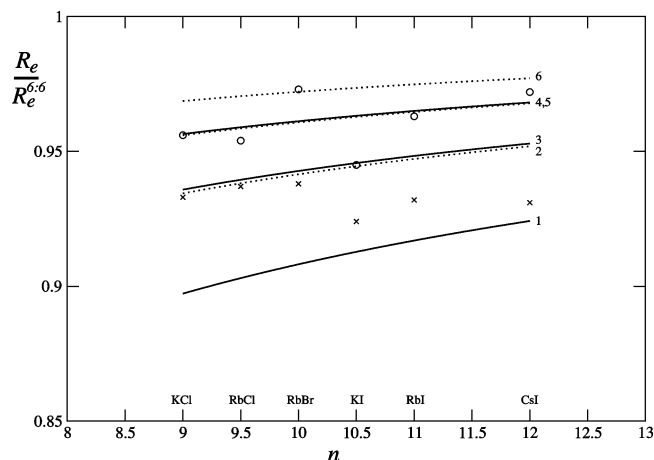
Figure 2. Predicted ratios of the optimum constrained $(a = b)$ separations in nanocrystals relative to the bulk. The lines are from Born model 54: solid lines are for the 1D system, and dotted lines are for the 2×1 crystal. $A = A_{6:6}$ for lines 1 and 2; lines 3 and 4 (dotted) have $f = 1.5$; lines 5 (solid) and 6 have $f = 3$. The crosses and circles are for the 1D crystals of indicated compositions. The crosses are derived from 54 and 53 using the f value taken from the ab initio computations, as described in section 3.2.1. The circles are derived by locating the R value minimizing the ab initio $U_{1D}(R)$ with inclusion of the dispersive attractions.

2.3. Difference between the Longitudinal and Transverse Separations. *2.3.1. Fundamental Equations and Deductions.* For the nanocrystals containing more than a single chain, it is useful to distinguish between the intra- and interchain contributions to the total Madelung energy $N_A U_{mad}(a, b)$. Although there are N_A/n_c cations in a nanocrystal composed of n_c chains, the total intrachain Madelung energy in a crystal having n_c chains is still given by $-N_A(2 \ln 2)/b$, unchanged from the single chain system. After defining the total interchain Madelung energy in 1 mol as $N_A U_{ic}^{mad}(a, b)$, the energy $U(a, b)$ in expression 1 for the cohesion becomes

$$U(a, b) = -\frac{2 \ln 2}{b} + U_{ic}^{mad}(a, b) + \frac{2A}{b^n} + \frac{CA}{a^n} \tag{7}$$

For the purposes of calculating $U_{ic}^{mad}(a, b)$, the relevant properties of any pairs of chains are specified by the integer q which yields the perpendicular distance between the two chains. This is the distance between two ions in the same plane, each of which lies in one of the two chains. If the ion in the second chain has x and y coordinates of ja and ka measured relative to the first ion, so that j and k are integers, then q is defined as $(j^2 + k^2)$, so that distance $a(j^2 + k^2)^{1/2}$ between the two ions is $a\sqrt{q}$. Table 1 presents all the q values arising in each nanocrystal. Since the two ions will have the same charge if q is even but opposite charges when q is odd, the electrostatic interaction energy of an ion in the first chain with the ion in the second chain is $(-1)^q/(a\sqrt{q})$. The distance between the ion in the first chain and one in the second, if the latter resides in a plane having z coordinate of mb relative to the first plane, is $(qa^2 + m^2b^2)^{1/2}$, where m is a positive integer. The electrostatic energy of interaction between these two ions is therefore $(-1)^{q+m}/(qa^2 + m^2b^2)^{1/2}$. The total electrostatic interaction energy of interaction between the one ion in the first chain with all ions in the second chain is therefore given by $(-1)^q/(a\sqrt{q})$ $+ 2\sum_{m=1}^{\infty}(-1)^{q+m}/(qa^2 + m^2b^2)^{1/2}$ because, for nonzero m, there are two planes located at a distance mb from the first plane. Since any chain contains N_A/n_c cations, the electrostatic interaction energy between all these cations in the first chain with all

Model for Properties of Nanocrystalline Ionic Solids

J. Phys. Chem. B, Vol. 110, No. 12, 2006 **5939**

the ions in the second chain is given by multiplying this energy by N_A/n_c. If there are n_{cp}^q pairs of chains of the type defined by q, the total electrostatic interaction in all chain pairs of the type q between all cations in the first chain in any pair with all other ions is given by a further multiplication by n_{cp}^q. The required total interchain Madelung energy $U_{ic}^{mad}(a, b)$ will be twice the energy already calculated in order to include the interaction of all anions, in the first chain in any of the pairs, with all other ions in the second chain in each pair. Hence, $U_{ic}^{mad}(a, b)$ is given by

$$U_{ic}^{mad}(a, b) = \frac{2}{n_c}\sum_q (-1)^q n_{cp}^q \left(\frac{1}{a\sqrt{q}} - 2\sum_{m=1}^{\infty}\frac{(-1)^{m+1}}{(qa^2 + m^2b^2)^{1/2}}\right) \quad (8)$$

The numbers n_{cp}^q of pairs of chains of the type q are presented in Table 1.

The factor $N_A(2/n_c)n_{cp}^1$ gives, for 1 mol, the number of electrostatic interactions between closest ion pairs, so that this equals the number of short-range repulsions. This provides an alternative derivation of the coefficient C in eq 7, showing it to take the value $(2/n_c)n_{cp}^1$.

It proves useful to introduce the definition of the ratio x of a to b by

$$x = \frac{a}{b} \quad (9)$$

which allows 8 to be written in the form

$$U_{ic}^{mad}(a, b) = -\frac{M_b(x)}{b} \quad (10)$$

where

$$M_b(x) = \frac{2}{n_c}\sum_q (-1)^{q+1} n_{cp}^q \left(\frac{1}{x\sqrt{q}} - 2\sum_{m=1}^{\infty}\frac{(-1)^{m+1}}{(qx^2 + m^2)^{1/2}}\right) \quad (11)$$

This allows $U(a, b)$ to be expressed as

$$U(a, b) = -\frac{2\ln 2 + M_b(x)}{b} + \frac{2A}{b^n} + \frac{CA}{a^n} \quad (12)$$

Since $M_b(x)$ is dimensionless being, for any given structural type, a function of solely the variable x, it can be regarded as a generalization of the Madelung constant that can be called the Madelung function.

The structures of the nanocrystals are best understood by first considering optimizing the geometry under the constraint that $a = b$, followed by elucidating any further changes that may result from removing this constraint. Any such constrained value of $b(= a)$ will be denoted R with the R minimizing $U(b, b)$ ($= U(R)$) denoted R_e. Noting that, for such constrained geometries, $M_b(x)$ becomes the constant $M_b(1)$ shows that

$$\frac{dU(R)}{dR} = \frac{2\ln 2 + M_b(1)}{R^2} - \frac{nA(2 + C)}{R^{n+1}} \quad (13)$$

Application of the condition $dU(R)/dR|_{R=R_e} = 0$ yields the relation

$$2\ln 2 + M_b(1) - \frac{nA(2 + C)}{R^{n-1}} = 0 \quad (14)$$

which shows R_e to be given by

$$R_e = \left(\frac{nA(2 + C)}{2\ln 2 + M_b(1)}\right)^{1/(n-1)} = \left(\frac{nA(2 + C)}{M_R}\right)^{1/(n-1)} \quad (15)$$

The quantity M_R, defined through the second equality (15) as $2\ln 2 + M_b(1)$ is just the Madelung constant for the constrained crystal. Division of eq 15 by result 5 for the separation $R_e^{6:6}$ in the bulk shows that

$$\frac{R_e}{R_e^{6:6}} = \left(\frac{2 + C}{6}\frac{M_{6:6}}{M_R}\right)^{1/(n-1)} \quad (16)$$

The values of $M_b(1)$ evaluated from eq 47, as described in section 3.1.1, are presented in Table 1. The value for the 2 × 1 crystal shows, as expected, that two chains attract, their interaction energy being $-0.116741/R$. However, this interchain attraction is much less than that of $-(2\ln 2)/R$ within a single chain. Examination of the top part of Figure 1 reveals the physical origin of this difference. Within any chain, each ion has two closest neighbors at a distance R and of opposite charge with the two closest neighbors of the same charge being located at the large distance of $2R$. However, not only does each ion have only one oppositely charged neighbor at a distance R in the adjacent chain, but also there are two neighbors of the same charge at a distance of $\sqrt{2}R$ in the other chain. For 1 mol of 2 × 2 crystal, although there are twice as many closest interchain attractions of energy $-0.116741/R$, the total interchain interaction energy is less than twice the value for the 2 × 1 crystal because each pair of chains separated by the distance $\sqrt{2}R$ repel rather than attract, these contributing $+0.02857/R$ to the Madelung energy. Examination of the bottom part of Figure 1 reveals the origin of this repulsion, the closest interaction at a distance $\sqrt{2}R$ being between two ions of the same charge. The values of $M_b(1)$ in Table 1 show that the ratio $M_{6:6}/(2\ln 2 + M_b(1))$, although greater than one, is always closer to unity than is the fraction $(2 + C)/6$. It then follows from 16 that the constrained (R_e) equilibrium separation is reduced compared to that of the bulk. Furthermore, on descending in Table 1, that is, on passing to nanocrystals with progressively larger cross sections, the Madelung energy ratio decreases less rapidly than the increase of the ratio $(2 + C)/6$. This shows that the fractional contraction of the constrained R_e from the bulk separation $R_e^{6:6}$ decreases with increasing nanocrystal cross section. For the 2 × 1 crystal, the dependence on n of ratio 16, equal to $0.5814^{1/(n-1)}$, is shown in Figure 2. Comparison of this result with that for the 1D chain shows that the latter exhibits the largest fractional contraction at fixed n. This therefore continues, to the limit, the trend of increasing fractional contraction with decreasing nanocrystal cross section.

The direction of the individual changes in a and b which lower the energy on relaxing the structure from the optimum constrained $a = b$, $x = 1$ geometry is determined by the signs of the two derivatives $dU(a, b)/da|_b$ and $dU(a, b)/db|_a$ when evaluated at $x = 1$. These derivatives are readily derived from 12 for all values of x by using the chain rule and noting that $dx/da|_b = 1/b$ and $dx/db|_a = -a/b^2$. The results are

$$\frac{dU(a, b)}{da}\Big|_b = -\frac{1}{b^2}\frac{dM_b(x)}{dx} - \frac{nCA}{a^{n+1}} \quad (17)$$

$$\frac{dU(a, b)}{db}\Big|_a = \frac{2\ln 2 + M_b(x)}{b^2} + \frac{a}{b^3}\frac{dM_b(x)}{dx} - \frac{2nA}{b^{n+1}} \quad (18)$$

Evaluation of these derivatives at the optimal constrained ($x = 1$) geometry for which $a = b = R_e$ and addition of the results show that

$$\left.\frac{dU(a, b)}{da}\right|_{a=b=R_e} + \left.\frac{dU(a, b)}{db}\right|_{a=b=R_e} =$$

$$\frac{2 \ln 2 + M_b(1)}{R_e^{\,2}} - \frac{nA(2 + C)}{R_e^{\,n+1}} = 0 \quad (19)$$

The last step, showing that the entire quantity 19 vanishes, follows because the expression on the right of the first equality sign is nothing but constrained equilibrium condition 14. Result 19 shows that one of the distances a or b must decrease on relaxing the structure from the constrained equilibrium geometry while the other increases. This shows that at least one of these distances must be less than the separation ($R_e^{6:6}$) in the bulk material.

2.3.2. Ratio between the Longitudinal and Transverse Separations. Comparison of ratio x ($= a/b$) with unity will determine which of the distances contracts on relaxing from the optimum constrained geometry. An equation for x is derived by writing the term CA/a^n in 12 as $(1/b^n)CA/x^n$, thus converting $U(a, b)$ into a function $U(x, b)$ of just the variables x and b. The two partial derivatives $dU(x,b)/db|_x$ and $dU(x, b)/dx|_b$, which are both zero at the optimal unconstrained geometry for which $b = b_e$ and $x = x_e$, are then found from 12 to be

$$\left.\frac{dU(x, b)}{db}\right|_x = \frac{2 \ln 2 + M_b(x)}{b^2} - \frac{nA(2 + Cx^{-n})}{b^{n+1}} \quad (20)$$

$$\left.\frac{dU(x, b)}{dx}\right|_b = -\frac{1}{b}\frac{dM_b(x)}{dx} - \frac{nCA}{b^n x^{n+1}} \quad (21)$$

The vanishing of 20 at the relaxed equilibrium geometry shows that

$$\frac{nA}{b_e^{\,n-1}} = \frac{2 \ln 2 + M_b(x_e)}{2 + Cx_e^{\,-n}} \quad (22)$$

Substitution of this relation into 21 shows, after noting that this also vanishes at the relaxed equilibrium geometry, that

$$-\frac{2 \ln 2 + M_b(x_e)}{\left.\dfrac{dM_b(x)}{dx}\right|_{x=x_e}} = x_e(1 + 2C^{-1}x_e^{\,n}) \quad (23)$$

Four interesting results plus a further useful inequality can be deduced from this relation. The useful inequality is that, since the three quantities ($2 \ln 2 + M_b(x_e)$), x_e, and C are necessarily positive, it follows that $dM_b(x)/dx|_{x=x_e}$ must be negative.

The first main deduction from 23 is that this shows that, given the structural type of the nanocrystal, the ratio of a/b is independent of the strength A of the short-range cation–anion repulsion with x_e being determined solely by the range of the potential as defined by the Born exponent n. This range decreases with increasing n.

The second main deduction from 23 is, as would be expected, that x_e is not unity for the nanocrystals. This follows after noting that for the bulk material, which is just the limit of the sequence of nanocrystals considered in Table 1 for which the planes consist of m_1 rows and columns as m_1 tends to infinity, 23 is satisfied for $x_e = 1$ with $C = 4$. Considering still the case of $x = 1$, the ratio on the left-hand side of 23 will be different for

different nanocrystals, all these ratios being different from that in the bulk, and moreover, this ratio will not vary with the nanocrystal as $1 + 2C^{-1}$. The right-hand side (RHS) of 23 depends only on the number of nearest neighbors and involves terms of short range while the left-hand side originates from the electrostatic interactions which, being of long range, involve the interactions of all the ions. These observations show that, for the nanocrystals, 23 will be satisfied by values of x_e that are not unity.

The third deduction follows from 23 by noting that while its left-hand side is independent of n, the right-hand side contains $x_e^{\,n}$ with the exponent n being a number no less than 6. Since it has already been shown that x_e will not be unity for a nanocrystal, the right-hand side of 23 will vary much more rapidly with x for fixed n than will the left-hand side. It therefore follows that, as n increases, a smaller deviation of x_e from unity is required to satisfy 23. This means that the relaxation of any nanocrystal from its optimal constrained geometry defined by 15 will decrease with increasing n.

The fourth deduction from 23 is the determination of the size of x when compared to unity. This determines whether, on relaxation from the optimal constrained geometry, a increases with b decreasing or vice-versa. On passing from the bulk upward from the bottom through the nanocrystal sequence in Table 1, the right-hand side of 23 has the values, $3/2$, $5/3$, $7/4$, 2, and 3 for $x = 1$. The magnitudes of $dM_b(x)/dx$ should be expected to follow $M_b(x)$ in decreasing with decreasing nanocrystal cross section and, moreover, to be roughly comparable with the $M_b(x)$. This shows that $-dM_b(x)/dx$ will be small compared with $2 \ln 2$ because the data in Table 1 show that the $M_b(x)$ values have this property. The values of the left-hand side of 23 evaluated for $x = 1$, therefore, increase more rapidly with decreasing nanocrystal cross section than does the factor $1 + 2/C$ already listed. This shows that since, for the bulk, 23 is satisfied with $x = 1$ with both sides equal to $3/2$, the left-hand side will become progressively larger than the right-hand side on traversing this sequence if x is kept at unity. For example, for the 2×1 crystal, evaluation of $dM_b(x)/dx|_{x=1}$ from 11 yields -0.426 which taken in conjunction with the $M_b(1)$ value in Table 1 leads to a value of 3.53 for the left side of 23. Since the right side of 23 contains x raised to the high power n, increasing x from unity will cause the right side to increase much more rapidly than the left side of 23 which contains only inverse powers of geometric parameters. Hence, 23 requires values of x, increasingly greater than unity, to be satisfied as one passes up through the sequence of nanocrystals in Table 1. It has therefore been shown that relaxation of any nanocrystal from its constrained equilibrium geometry will cause b to decrease while a increases. This result is readily understood physically as being a consequence of the Coulombic binding within each chain being much greater than that between different chains.

2.3.3. Interchain Coulomb Energy and Nanocrystal Relaxation. Result 18, when taken in conjunction with both the corresponding derivatives of relation 2 for energy of a 1D chain, yields expressions which show how the interchain coulomb energy varies as the crystal structure is relaxed toward its equilibrium structure. Division of eq 4 by eq 15 yields

$$\frac{b_e^{1D}}{R_e} = \left(\frac{2}{(2 + C)}\frac{M_R}{2 \ln 2}\right)^{1/(n-1)} \quad (24)$$

Since the ratio $M_R/(2 \ln 2)$ is closer to unity than is $2/(2 + C)$, result 24 shows that, in any nanocrystal having a cross section

Model for Properties of Nanocrystalline Ionic Solids

J. Phys. Chem. B, Vol. 110, No. 12, 2006 **5941**

of two or more chains, its constrained equilibrium separation R_e is greater than that b_e^{1D} in the 1D system. The observation that, for all distances b greater than b_e^{1D} in the 1D system, the derivative $dU_{1D}(b)/db$ of 2 will be positive shows that

$$\frac{2 \ln 2}{b^2} - \frac{2An}{b^{n+1}} > 0, \quad \text{for all } b > b_e^{1D} \tag{25}$$

This shows from 18 that, since $dU(a, b)/db|_{a=a_e, b=b_e}$ is zero,

$$M_b(x_e) + \frac{a_e}{b_e} \frac{dM_b(x)}{dx}\bigg|_{x=x_e} < 0 \tag{26}$$

This is consistent with the deduction from 23 that $dM_b(x)/dx|_{x=x_e}$ is negative.

Both result 26 and the established sign of $dM_b(x)/dx|_{x=x_e}$ are significant because it follows from 10 that

$$\frac{dU_{ic}^{mad}(a, b)}{da}\bigg|_b = -\frac{1}{b^2} \frac{dM_b(x)}{dx} \tag{27}$$

and

$$\frac{dU_{ic}^{mad}(a, b)}{db}\bigg|_a = \frac{1}{b^2}\left(M_b(x) + \frac{a}{b} \frac{dM_b(x)}{dx}\right) \tag{28}$$

The negative sign of $dM_b(x)/dx$ shows that 27 is positive, which means that the electrostatic energy is raised by an increase of a. This confirms, as expected, that the chains are bound by their total mutual Coulombic attraction, as already elucidated in the discussion after eq 16. However, it follows from 28, when taken in conjunction with 26, that a decrease of b which lowers the total electrostatic energy actually increases the total interchain electrostatic interaction. This can be understood from Figure 1 (top) from which it is seen that if b is decreased while keeping a fixed, the distance between the nearest like pairs of ions in different adjacent chains is decreased thereby raising the total interchain electrostatic energy even though these chains still attract by virtue of the attraction between the closest pairs of unlike ions in the different chains. Thus, it is the increasingly negative electrostatic interaction energy $-(2 \ln 2)/b$ within the chains which causes the value of b to decrease on relaxing a nanocrystal from its constrained equilibrium geometry. This energy is significantly greater in magnitude than the total interchain electrostatic interaction energy as shown by the values of $M_b(1)$ reported in Table 1 when compared with $2 \ln 2$.

2.3.4. Ultra-Short-Range Limit of Very High n. The ratio x will be quite close to unity. This suggests that it is useful to define the deviation, ϵ, of x from 1 by

$$x = 1 + \epsilon \tag{29}$$

and then to obtain an expression for ϵ correct to first order. This procedure defines the two constants G and H through

$$-\frac{2 \ln 2 + M_b(x_e)}{\dfrac{dM_b(x)}{dx}\bigg|_{x=x_e}} = G + H\epsilon \tag{30}$$

The derivation of numerical values for G and H is described in section 3. Introducing both definitions 29 and 30 into 23 transforms this relation into

$$G + H\epsilon = (1 + \epsilon) + 2C^{-1}(1 + \epsilon)^{n+1} \tag{31}$$

which on a simple rearrangement yields

$$(1 + \epsilon)^{n+1} = \frac{C}{2}[(G - 1) + \epsilon(H - 1)] \tag{32}$$

It is useful to introduce the two further constants defined by

$$k_1 = \frac{H - 1}{G - 1} \tag{33}$$

and

$$k_2 = \frac{C}{2}(G - 1) \tag{34}$$

After expressing 32 in terms of the variables defined by 33 and 34 and taking the $n + 1$ root of both sides, a Taylor expansion of the resulting factor of $(1 + k_1\epsilon)^{1/(n+1)}$ to first-order in ϵ yields the result

$$\epsilon\left(1 - \frac{k_1 k_2^{1/(n+1)}}{n + 1}\right) = k_2^{1/(n+1)} - 1 \tag{35}$$

Result 35 first shows that ϵ decreases as n increases so that x becomes increasingly close to unity with increasing n, thus confirming the result already deduced from 23. However, 35 immediately shows that ϵ tends to zero as n tends toward infinity, thus showing that there will be no relaxation from the constrained equilibrium geometry in the limit that the ions behave as hard spheres, this corresponding to infinite n. This limiting result is not readily deduced directly from form 23. The development from 32 to 35 is needed because the limit of large n is not accessible if a Taylor expansion is applied to the left-hand side of 32 and only the two leading terms are retained.

3. Numerical Results for Structural Trends

3.1. Predictions from the Basic Born Type Model. *3.1.1. Approximate Analytic Equation.* A Madelung function $M_b(x)$ contains one of more infinite sums which are functions of the one variable $t = qx^2$. Each such sum, to be denoted $S(t)$, is defined by

$$S(t) = \sum_{m=1}^{\infty} \frac{(-1)^{m+1}}{(t + m^2)^{1/2}} \tag{36}$$

thereby allowing $M_b(x)$ to be expressed as

$$M_b(x) = \frac{2}{n_c}\sum_q (-1)^{q+1} n_{cp}^q\left(\frac{1}{x\sqrt{q}} - 2S(qx^2)\right) \tag{37}$$

The observation that the large m terms in the sum on the RHS of 36 tend to $(-1)^{m+1}/m$, which is just the expansion of $\ln 2$, suggests that $S(t)$ might be accurately approximated by the analytic form

$$S_{an}(t) = D + \frac{E \ln 2}{(1 + t)^k} \tag{38}$$

where D, E, and k are constants to be determined. The exact results from 36 that $S(0) = \ln 2$ and $S(\infty) = 0$ show that one must take $D = 0$ and $E = 1$ in 38. The value of k is determined by demanding that the exact result for $dS(t)/dt|_{t=0}$ derived from

$$\frac{dS(t)}{dt} = -\frac{1}{2}\sum_{m=1}^{\infty}\frac{(-1)^{m+1}}{(t+m^2)^{3/2}} \quad (39)$$

is exactly reproduced by the corresponding result derived by differentiating 38 with respect to t. This procedure shows that k must take the value 0.65032557. Although evaluation of sum 39 by direct summation is rapidly convergent, this is not the case for the original sums $S(t)$ which were required to derive the numerical results for $M_b(1)$ presented in Table 1. These sums are most readily evaluated by writing

$$S(t) = \sum_{m=1}^{\infty}\frac{(-1)^{m+1}}{m} + \sum_{m=1}^{\infty}(-1)^{m+1}\left(\frac{1}{(t+m^2)^{1/2}} - \frac{1}{m}\right) \quad (40)$$

$$= \ln 2 + \sum_{m=1}^{\infty}(-1)^{m+1}\left(\frac{1}{(t+m^2)^{1/2}} - \frac{1}{m}\right) \quad (41)$$

The sum remaining on the right side of 41 converges rapidly when explicitly evaluated for the small t values of interest here ($t \le 1.3 \times 3\sqrt{2}$). The alternative approach of demanding that 38 precisely reproduces the exact result when $t = 1$ yields a k value of 0.6522, very similar to that already deduced.

The pth derivatives of exact form 36 and its analytic approximation 38 with $D = 0$ and $E = 1$ are

$$\frac{d^pS(t)}{dt^p} = \frac{(-1)^p(2p-1)!!}{2^p}\sum_{m=1}^{\infty}(-1)^{m+1}\left(\frac{1}{(t+m^2)^{p+1/2}}\right) \quad (42)$$

and

$$\frac{d^pS_{an}(t)}{dt^p} = \frac{(-1)^pk(k+1)...(k+p-1)\ln 2}{(1+t)^{k+p}} \quad (43)$$

The quantity $(2p-1)!!$ is defined as 1, 3, 5, ..., $(2p-1)$. The agreement of the results of 0.7439, 1.9716, and 7.1971 derived from 43 at $t = 0$ for $p = 2$, 3, and 4, respectively, with the corresponding exact values of 0.7291, 1.8611, and 6.5499 derived by evaluating 42 shows that one can expect the analytic form for $S(t)$ to be sufficiently accurate for all the t values of interest that are used both in 23 and in the evaluation of the first derivative in that relation that only insignificant errors are introduced into either the x_b values thereby derived or those of the cohesive energies discussed in section 4.

Substitution into 37 of 38 with $D = 0$, $E = 1$, and $k = 0.65032557$ yields an analytic result for $M_b(x)$ in the form

$$M_b(x) = \frac{2}{n_c}\sum_q(-1)^{q+1}n_{cp}^q\left(\frac{1}{x\sqrt{q}} - \frac{2\ln 2}{(1+qx^2)^k}\right) \quad (44)$$

Introduction of the definitions

$$G_x = \frac{2}{n_c}\sum_q\frac{(-1)^{q+1}n_{cp}^q}{\sqrt{q}} \quad (45)$$

and

$$G_q = \frac{2}{n_c}(-1)^{q+1}n_{cp}^q \quad (46)$$

allows $M_b(x)$ to be written as

$$M_b(x) = \frac{G_x}{x} - \sum_q G_q\frac{2\ln 2}{(1+qx^2)^k} \quad (47)$$

which is the basic result of this section. The numerical values of constants G_x and G_q reported in Table 2 enable $M_b(x)$ to be evaluated for all nanocrystals. Since 47 can be analytically differentiated with respect to x, the eq 23 determining x can be written in a closed form which can be readily solved. Result 47 also allows the constants H, G, k_1, and k_2 in the linearized form of 23 (35) to be evaluated.

3.1.2. Solution for Structural Trends. It is of interest to examine the nanocrystal dependence of the derivatives of the energy with independent variations of a and b evaluated at the constrained equilibrium geometry. These will give an indication of the relative strengths of the forces driving the crystal away from the latter configuration. The expressions used to evaluate $dU(a, b)/da|_{a=b=R_e}$ and $dU(a, b)/db|_{a=b=R_e}$ are derived by setting $a = b = R_e$ in general results 17 and 18 and then using result 14 to eliminate the terms A/R_e^{n-1} from the derivatives. The result for $dU(a, b)/da|_{a=b=R_e}$ is

$$\frac{dU(a, b)}{da}\bigg|_{a=b=R_e} = -\frac{1}{R_e^2}\left(\frac{dM_b(x)}{dx}\bigg|_{x=1} - \frac{M_RC}{2+C}\right) = -\frac{K_e}{R_e^2} \quad (48)$$

The derivation of an expression for $dU(a, b)/db|_{a=b=R_e}$ by using the same procedure yields a result which is just the negative of eq 48. This provides a very specific illustration of relation 19. Numerical values for the coefficient K_e in each of the nanocrystals are presented in Table 3. Although these coefficients are independent of n, the dependence on n in the expression for R_e means that the gradients of 48 are not entirely independent of n. The result that these gradients increase with decreasing nanocrystal cross section strongly suggests that the smaller nanocrystals will exhibit greater relaxations from the optimal constrained geometry.

The ratios a_e/b_e predicted by numerical solution of 23 with $M_b(x)$ expressed as in 47 are presented in Table 4 for four different values of n. The results confirm the previous analysis that these ratios are all greater than unity, that they decrease with increase of both n and the size of the nanocrystal cross section. The 2×1 nanocrystal with $n = 6$, the value for LiF, shows the largest distortion from the bulk, this being almost 11%. This is reduced to 2.9% for the 4×4 LiF crystal. The 4×4 crystal with $n = 12$, the value for CsI, shows the smallest distortion of a mere 0.7%. The fractional contractions $b_e/R_e^{6:6}$ of the interplane distances relative to the bulk were calculated from the relation

$$\frac{b_e}{R_e^{6:6}} = \left(\frac{2+Cx^{-n}}{6}\frac{M_{6:6}}{2\ln 2 + M_b(x)}\right)^{1/(n-1)} \quad (49)$$

derived by using 5 to both introduce the bulk separation and to eliminate A from 22. The results, presented in Table 4, again show that the fractional contractions of b_e decrease with increase of either n or the nanocrystal cross section. These contractions range from 16% for the 1D LiF system to 1.7% for the 4×4 CsI crystal. The fractional distortions $a_e/R_e^{6:6}$ of a relative to the bulk, derived from the results in Table 4 as $(a_e/b_e)b_e/R_e^{6:6}$, are naturally smaller than those of the interplane separations. However, the results show that a_e also is predicted to be contracted, albeit slightly, relative to the bulk. These fractional contractions cover a much more narrow range, from 3.4% for the 2×1 LiF system to 1% for the case of 4×4 CsI. Since a_e

Model for Properties of Nanocrystalline Ionic Solids

J. Phys. Chem. B, Vol. 110, No. 12, 2006 **5943**

TABLE 2: Coefficients G_q and G_x Yielding the Madelung Function $M_b(x)$ through Equation 47

crystallite	G_q	G_x
2×1	$G_1 = 1$	1
2×2	$G_1 = 2, G_2 = -1$	$\left(2 - \dfrac{1}{\sqrt{2}}\right)$
3×3	$G_1 = {}^8/_3, G_2 = -16/9, G_4 = -{}^4/_3, G_5 = 16/9, G_8 = -{}^4/_9$	$\left(2 - \dfrac{2}{\sqrt{2}} + \dfrac{16}{9\sqrt{5}}\right)$
4×4	$G_1 = 3, G_2 = -{}^9/_4, G_4 = -2, G_5 = 3, G_8 = -1, G_9 = 1,$ $G_{10} = -{}^3/_2, G_{13} = 1, G_{18} = -{}^1/_4$	$\left(\dfrac{7}{3} - \dfrac{17}{6\sqrt{2}} + \dfrac{3}{\sqrt{5}} - \dfrac{3}{2\sqrt{10}} + \dfrac{1}{\sqrt{13}}\right)$

TABLE 3: Coefficients K_e of Equation 48

crystallite	K_e
2×1	0.0754
2×2	0.0632
3×3	0.0585
4×4	0.0230

TABLE 4: Ratios a_e/b_e and $b_e/R_e^{6:6}$ for Four Different Values of Born Exponent n

	$n = 6$		$n = 9$		$n = 10.5$		$n = 12$	
crystallite	a_e/b_e	$b_e/R_e^{6:6}$	a_e/b_e	$b_e/R_e^{6:6}$	a_e/b_e	$b_e/R_e^{6:6}$	a_e/b_e	$b_e/R_e^{6:6}$
1×1		0.841		0.897		0.913		0.924
2×1	1.107	0.872	1.045	0.922	1.035	0.935	1.028	0.944
2×2	1.074	0.910	1.031	0.948	1.024	0.957	1.019	0.963
3×3	1.039	0.942	1.016	0.968	1.012	0.973	1.010	0.977
4×4	1.029	0.956	1.012	0.976	1.009	0.980	1.007	0.983
bulk	1.000	1.000	1.000	1.000	1.000	1.000	1.000	1.000

is always larger than b_e, the former distance recovers more quickly toward the bulk separation $R_e^{6:6}$ as the nanocrystal cross section increases.

Evidence that the predictions in Table 4 are trustworthy is provided by the results of ab initio Hartree−Fock computations[20] of the electronic structures of 2×2 LiF nanocrystals. These were performed with the numbers of planes being progressively increased until the geometries of the planes near the centers of the small crystallites remained unchanged on the addition of further planes. These computations, to be reported in detail elsewhere, predicted $a_e = 3.685$ au and $b_e = 3.458$ au, thereby yielding an a_e/b_e ratio of 1.066 in good agreement with that of 1.074 derived from the present Born type model. Furthermore, both these results are smaller than the separation of 3.789 au (ref 21) predicted by a Hartree−Fock computation with periodic boundary conditions for the bulk system. Combination of this result with that for in the 2×2 system yields a value of 0.912 for $b_e/R_e^{6:6}$, in excellent agreement with that of 0.910 predicted from the Born type model. The ab initio computations included not only all the physical effects described in the present analytical method but also the short-range interactions between non-nearest ion pairs, of which the anion−anion term will be the least small, as well as third and higher order multibody effects of the short-range Löwdin type.[22] The agreement of the analytic model with the ab initio results provides evidence that the additional effects included in the latter play only a very minor role in determining the structures of the nanocrystals, at least for LiF. These computations are also comparable in that neither of the two sets include the interionic dispersive attractions.

Further evidence that the present Born model captures the essential physics is provided by the computation using the GULP program[23] of the structure of a 2×2 CsI nanocrystal, this being infinite in extent through the use of the periodic boundary

TABLE 5: Coefficients k_1 and k_2 of General Linearized Equation 35

crystallite	k_1	k_2
2×1	4.540	1.266
2×2	4.732	1.172
3×3	4.910	1.084
4×4	5.022	1.059

conditions. The interionic pair potentials required for this program were computed using the relativistic integrals program.[24,25] This method, after augmentation with descriptions of both the short-range electron correlation and the interionic dispersive attractions, has been shown to provide a good description of bulk ionic crystals[26−29] including the delicate problem of the relative stabilities of the 6-fold and 8-fold coordinated phases of cesium chloride.[30,31] The methodology is described in the following publications: refs 26, 28, 32, and 33. The computations for the 2×2 nanocrystal predicted a_e/b_e and $b_e/R_e^{6:6}$ ratios of 0.973 and 1.004 in reasonable agreement with the Born model values of 0.963 and 1.019. This comparison is less clear-cut than the one for LiF just described because the GULP computations included dispersion which is not explicitly included in the Born model, this only entering the latter indirectly, if at all, through the derivation of the value of 12 for n from the experimental compressibilities.

The numerical values of the coefficients k_1 and k_2 needed to evaluate x_e as $1 + \epsilon$ using the linearized approximation to 23 (35) are reported in Table 5. For a 4×4 nanocrystal, this predicts values of 0.0297 and 0.00722 for $n = 6$ and 12, respectively, in very good agreement with the results of 0.00292 and 0.00716 (Table 4) derived from 23. For 2×1 nanocrystals, the corresponding linearized results of 0.10074 and 0.0275 for $n = 6$ and 12 are also in good agreement with those of 0.10687 and 0.0283 derived from 23.

3.2. Influence of the Finer Details of the Cation−Anion Interaction. *3.2.1. Structural Dependence of the Effective Cation−Anion Repulsion.* It has been assumed that the quantity A defining the strength of the short-range cation−anion interaction is independent of structure. In this section, the consequences of any possible such variations and their origins are examined. It is now well established that, although the properties of cations in a crystal remain essentially unchanged from those of the free cation, anions are significantly modified from their free states on entering a crystal.[26,28,32−37] In particular, in-crystal anions are slightly but significantly compressed relative to free anions. This compression means that the cohesive energy $[U(R)]$ for $x = 1$ is given, in the leading approximation of neglecting both the interionic dispersive attractions and the short-range interactions between more distant pairs of ions, by

$$U(R) = -\frac{M_R}{R} + E_{re}(R) + (2 + C)V_s(R) \qquad (50)$$

Here, $E_{re}(R)$ is the rearrangement energy required to convert the free anion into its form optimal for the crystal with the specified geometry while $V_s(R)$ is, for cation−anion separation R, the short-range energy of interaction of one cation with one anion measured not with respect to the sum of the energies of the free ions but with respect to the sum of the free cation energy and the energy that an isolated anion would have if it had the wavefunction optimal for the crystal with that geometry.[30−33] Result 50 shows that the cation−anion repulsions, which are represented in the standard Born model as AR^{-n}, are actually effective potentials $V_{eff}(R)$ given by

$$V_{eff}(R) = V_s(R) + \frac{E_{re}(R)}{2 + C} \tag{51}$$

because this definition allows 50 to be written as

$$U(R) = -\frac{M_R}{R} + (2 + C)V_{eff}(R) \tag{52}$$

It is this form, rather than 50, which is the standard expression for the cohesive energy in which no rearrangement energy appears explicitly.

Result 51 shows that $V_{eff}(R)$ will be structure dependent even if the individual terms $E_{re}(R)$ and $V_s(R)$ were independent of structure. The asumption that $V_{eff}(R)$ can be written in the Born form AR^{-n} implies that its two components in 51 also take this form. In the case that these two components are structure independent and vary as AR^{-n}, the ratio $E_{re}(R)/V_s(R)$ will be a constant, denoted as f, independent of R. It then follows from 51 that the term A entering expression 15 for the optimal constrained nanocrystal geometry will differ from that, to be designated $A_{6:6}$, appearing in result 5 for the separation in the bulk. It follows from 51 that

$$\frac{A}{A_{6:6}} = \left(1 + \frac{f}{2 + C}\right)\frac{1}{1 + \frac{f}{6}} \tag{53}$$

Division of eq 15 by eq 5 then yields

$$\frac{R_e}{R_e^{6:6}} = \left(\frac{A}{A_{6:6}}\right)^{1/(n-1)}\left(\frac{M_{6:6}}{M_R}\frac{2 + C}{6}\right)^{1/(n-1)} \tag{54}$$

Since the quantity C increases with increasing nanocrystal cross section, 53 shows that A will increase with decreasing cross section. It then follows from the presence in 54 of the additional factor of $(A/A_{6:6})^{1/(n-1)}$, greater than unity and absent from 16, that this crystal dependence of A will act to reduce the contraction predicted from 16.

More quantitative information can only be obtained by performing some electronic structure computations which yield numerical values for either $V_{eff}(R)$ or $E_{re}(R)$ and $V_s(R)$. For a range of bulk alkali halides, the two latter energies have been derived by augmenting the predictions computed with the relativistic integrals program (RIP)[24,25] with much smaller contributions arising from electron correlations of short range.[32] The results for both the 6:6 and 8:8 phases of CsCl have already been reported,[30,31] while the further results for KCl, RbCl, RbBr, KI, RbI, and CsI have not yet been published. These computations showed that $E_{re}(R)$ is typically about $1−1.5$ times larger than $V_s(R)$ although, of course, the latter makes the larger contribution to $V_{eff}(R)$ on account of the $2 + C$ denominator in 51. Furthermore, for many crystals, this ratio is found to be roughly independent of R, thereby enabling the constant f to be

TABLE 6: Ratio $b_e^{1D}/R_e^{6:6}$ Predicted from 54 and 53 (Born) with the Constant f Derived from the RIP Computations Compared with Those (RIP) Deduced Directly without Taking f to Be Constant

method	KCl	RbCl	RbBr	KI	RbI	CsI	CsCl
Born	0.930	0.935	0.940	0.935	0.943	0.951	0.964
RIP	0.933	0.937	0.938	0.924	0.932	0.931	0.952

defined. For the 1D chain and 2×1 nanocrystals, for which C is respectively zero and unity, ratio 53 takes the values $^7/_5$ and $^6/_5$ for $f = 1.5$. For the case of $f = 3$, these ratios are increased to $^5/_3$ and $^4/_3$. These results then show that distance ratio 54 becomes $(0.58828)^{1/(n-1)}$ and $(0.7003)^{1/(n-1)}$ for the 1D chains having $f = 1.5$ and 3, respectively, while the corresponding values for the 2×1 nanocrystal are $(0.69761)^{1/(n-1)}$ and $(0.7751)^{1/(n-1)}$. These predictions of 54 are compared in Figure 2 with those derived taking A to be independent of structure. The results illustrate the increase of $R_e/R_e^{6:6}$ toward unity with increase of f, n, and C.

For each of the 1D chains, for which R_e is designated as b_e^{1D}, the ratio $b_e^{1D}/R_e^{6:6}$ predicted from 53 and 54 using the value of f derived for the RIP computation for the R value near to the bulk experimental equilibrium is presented in the first line of Table 6 and plotted in Figure 2. For KCl, RbCl, and RbBr, the results lie close to the line for $f = 1.5$ because the RIP computations at near equilibrium geometries predicted f to be 1.27, 1.34, and 1.31, respectively. The results for the iodides lie appreciably below the $f = 1.5$ line because the RIP computations predicted smaller f values of 1.0, 1.1, and 1.3, respectively. For the 1D chains, it was straightforward to dispense with the assumption that f is independent of b by evaluating $U_{1D}(b)$ as a function of b from the values of $E_{re}(R)$ and $V_s(R)$ taken directly from the RIP computation for the bulk material. The resulting predictions for $b_e^{1D}/R_e^{6:6}$ are presented in the second line of Table 6. For KCl, RbCl, and RbBr, the results agree closely with those derived using the constant f assumption and presented in the first line. Examination of the computed values of $E_{re}(R)$ and $V_s(R)$ showed that their ratio depended only very weakly on R. For the iodides, however, this ratio varied significantly with R, being, for example, in the case of KI, 0.997 at $R = 6.7$ au but 0.859 at $R = 7.0$ au. Such variations explain why the $b_e^{1D}/R_e^{6:6}$ ratios derived using the constant f assumption do not agree with those computed directly using the RIP results for all distances.

For the crystals having more than one chain, result 49 for $b_e/R_e^{6:6}$ is modified in the same way as 54 in the event that the structural dependence of A is governed by 53 with $V_{eff}(R)$ taking the Born form. Thus, 49 acquires the additional factor of $(A/A_{6:6})^{1/(n-1)}$ which is introduced from 5 in using this both to introduce $R_e^{6:6}$ and to eliminate A from 22. This shows that the contractions predicted under the constant A assumption are increased although $b_e/R_e^{6:6}$ remains less than unity. For the 2×1 nanocrystal, the resulting predictions are compared in Table 7 with those derived assuming A to be constant.

The results presented in Figure 2 and Tables 6 and 7 were derived assuming that both $E_{re}(R)$ and $V_s(R)$ remained unchanged on passing from the bulk to the nanocrystal. The plausibility of this assumption can be tested by examining the variations of these quantities on passing from the 4-coordinated zinc blende structured polymorphs of the bulk crystals to those having the rock-salt or cesium chloride structures. Increase of the coordination number will tend to produce increasingly compressed anions, leading to greater rearrangement energies $E_{re}(R)$ but smaller short-range cation−anion repulsions $V_s(R)$. Such varia-

Model for Properties of Nanocrystalline Ionic Solids

J. Phys. Chem. B, Vol. 110, No. 12, 2006 **5945**

TABLE 7: Ratio of $b_e/R_e^{6:6}$ Computed for the 2 × 1 Crystallite Chain for Three Different Values of Born Exponent n and Parameter A Corresponding to $f = 0$, 1.5, and 3

	$b_e/R_e^{6:6}$		
n	$A^{2\times1} = A$	$A^{2\times1} = \frac{6}{5}A$	$A^{2\times1} = \frac{4}{3}A$
9	0.922	0.944	0.956
10.5	0.935	0.953	0.964
12	0.944	0.960	0.969

tions will tend to reduce the differences between the effective potentials in different phases of the same material when compared with those that would arise if $E_{re}(R)$ and $V_s(R)$ were both phase independent when the phase dependence of $V_{eff}(R)$ is caused solely by the factor of $1/(2 + C)$ multiplying the rearrangement energy in 51. Although the results[30,31] for CsCl showed that the change in $V_{eff}(R)$ on passing from the 6:6 to the 8:8 phase was significantly greater than that of its two components $E_{re}(R)$ and $V_s(R)$, the opposite was the case for all the other alkali halides mentioned above because, for these latter halides, both $E_{re}(R)$ and $V_s(R)$ were significantly more phase dependent than $V_{eff}(R)$. This shows that the results of this section are certainly relevant to any future measurements of the structure of the already prepared encapsulated CsCl system.[14] However, for the iodides, for which there is the most experimental data, the results indicate that the assumption that A remains unchanged on passing from the bulk to the encapsulated nanocrystal might not be less realistic than any derived under the assumption that it is $E_{re}(R)$ and $V_s(R)$ which remain unchanged.

3.2.2. Significance of the Dispersive Attractions. The Born model does not explicitly consider the dispersion forces between the ions. However, this model includes these implicitly, at least in some average way, through the introduction of both the experimental lattice constants and n values derived from the experimental compressibilities. The purpose of this section is to examine whether the previous conclusions would be significantly modified by explicitly introducing the interionic dispersive attractions. The essential features can be revealed by examining the 1D chain. These attractions are of much longer range than the short-range cation−anion repulsions. Thus, the leading, dipole−dipole, terms in the total dispersive attraction depend on the inverse sixth power of the interionic separations for distances sufficiently large such that dispersion damping[32,33,38] caused by ion wavefunction overlap can be neglected. It is therefore necessary to consider the dispersive attractions between all ion pairs and not just the closest neighboring pairs. In the leading approximation, one considers only the dipole−dipole dispersive interactions in their undamped form and neglects the smaller higher order contributions which commence with the dipole−quadrupole dispersive attractions. The total interionic dispersive attraction, $N_A U_{disp}(R)$ of 1 mol of a 1D, or bulk, crystal with geometry defined by the single closest neighbor separation R is then given by[32,33,39]

$$U_{disp}(R) = -R^{-n}\Big(S_6(CA)C_6(CA) +$$

$$\frac{1}{2}\{S_6(CC)[C_6(CC) + C_6(AA)]\}\Big) \quad (55)$$

The distance b in the 1D case is temporarily designated as R so that the exactly comparable equations can be written for the 1D and bulk systems. In 55, $C_6(XY)$, where X or Y can be either cation C or anion A, is the distance independent dipole−dipole dispersion coefficient which yields the attraction of one ion of type X with one of type Y separated by a distance r_{XY} as

$-C_6(XY)/r_{XY}$. Each dimensionless coefficient $S_6(XY)$ is the sum of the inverse sixth powers of the distances of all ions of type Y from one ion X, with all distances scaled such that R is unity. Thus, $-S_6(XY)C_6(XY)R^{-n}$ is the total dispersive attraction of one ion of type X with all other ions of type Y in the crystal. For any cation in the 1D chain, one anion is located at all distances which are odd multiples of the basic separation R, so that there are two such anions for any given distance defined regardless of direction. Similarly for any ion of type X, another ion of the same type is located any distance which is an even multiple of R. This shows that

$$S_6^{1D}(CA) = 2\sum_{n=1}^{\infty}\frac{1}{(2n-1)^6} = 2.0029 \quad (56)$$

and

$$S_6^{1D}(CC) = S_6^{1D}(AA) = 2\sum_{n=1}^{\infty}\frac{1}{(2n)^6} = 0.0318 \quad (57)$$

For the bulk rock-salt structure, it is a long established standard result that $S_6(CA) = 6.5952$ and that $S_6(CC) = S_6(AA) = 1.8067$.[33,39] It is useful to introduce the quantities T_6 defined as

$$T_6 = \frac{S_6(CA)C_6(CA) + \frac{1}{2}(S_6(CC)[C_6(CC) + C_6(AA)])}{2 + C} \quad (58)$$

It follows from the above values of the $S_6(XY)$ coefficients that

$$T_6^{1D} = 1.00145C_6(CA) + 0.00795[C_6(CC) + C_6(AA)] \quad (59)$$

and

$$T_6^{6:6} = 1.0092C_6(CA) + 0.1506[C_6(CC) + C_6(AA)] \quad (60)$$

The coefficients of 58 are useful because these enable the total cohesive energy to be expressed in the form

$$U(R) = -\frac{M_R}{R} + (2 + C)[AR^{-n} - T_6R^{-6}] \quad (61)$$

This differs from the expression for the cohesive energy of a nanocrystal in any constrained ($x = 1$) structure only in that the non-Coulombic interaction AR^{-n} between nearest neighbor ions has been replaced by an effective interaction $AR^{-n} - T_6R^{-6}$. For the 1D and bulk crystals, the factor $2 + C$ reduces to 2 and 6, respectively, just the coordination number of each ion. Differentiation of 61 with respect to R, equating the result to zero and then writing one resulting piece, $(nA(2 + C))/R_e^{n+1}$, in terms of the remainder yields the relation

$$R_e^{n-1} = \frac{nA(2 + C)}{M_R + 6(2 + C)T_6R_e^{-5}} \quad (62)$$

Division of this result for the 1D chain by the corresponding result for the bulk yields

$$\left(\frac{b_e^{1D}}{R_e^{6:6}}\right)^{n-1} = \frac{1}{3}\frac{M_{6:6} + 36T_6^{6:6}(R_e^{6:6})^{-5}}{2\ln 2 + 12T_6^{1D}(b_e^{1D})^{-5}} \quad (63)$$

where R_e for the 1D chain has been redesignated as b_e^{1D}. Comparison of this result with the corresponding ratio $(^1/_3)M_{6:6}/(2\ln 2)$ predicted without considering the dispersion

is achieved by defining the quantity δ as

$$\frac{3T_6^{6:6}(R_e^{6:6})^{-5}}{T_6^{1D}(b_e^{1D})^{-5}} = 3\frac{T_6^{6:6}}{T_6^{1D}}\left(\frac{b_e^{1D}}{R_e^{6:6}}\right)^5 = \frac{M_{6:6}}{2\ln 2} + \delta \qquad (64)$$

It then follows that one can write

$$\frac{M_{6:6} + 36T_6^{6:6}(R_e^{6:6})^{-5}}{2\ln 2 + 12T_6^{1D}(b_e^{1D})^{-5}} =$$

$$\frac{M_{6:6}\left(1 + \dfrac{12T_6^{1D}(b_e^{1D})^{-5}}{2\ln 2}\right) + 12T_6^{1D}(b_e^{1D})^{-5}\delta}{2\ln 2\left(1 + \dfrac{12T_6^{1D}(b_e^{1D})^{-5}}{2\ln 2}\right)} \qquad (65)$$

which will be greater than $M_{6:6}/(2\ln 2)$ if δ is positive. Since the dispersion is not the major term, it is sufficient to evaluate the ratio in 64 by using result 6 derived by considering only the Madelung and short-range repulsion. The smallest value predicted for the ratio $(b_e^{1D}/R_e^{6:6})^5$ is 0.4843, which is the result for $n = 7$. This shows that $3(b_e^{1D}/R_e^{6:6})^5$ must be greater than 1.4529, which shows that $3(T_6^{6:6}/T_6^{1D})(b_e^{1D}/R_e^{6:6})^5$ must also be greater than 1.4529 because it follows from results 59 and 60 that $T_6^{6:6}$ is greater than T_6^{1D}. Since this value is greater than that 1.2606 of $M_{6:6}/(2\ln 2)$, it follows that δ is positive and, hence, that the ratio of distances 63 will be greater than that predicted without considering the dispersive attractions.

The cohesive energies $U_{1D}(b)$ were calculated as function of b by using the RIP values of $E_{re}(R)$ and $V_s(R)$ computed for the bulk with the $C_6(XY)$ dispersion coefficients derived from the Slater−Kirkwood formula via the experimental molar polarizabilities, as described elsewhere. These computations included the dispersion damping[32,33,38] as well as the dipole−quadrupole dispersive attractions, both evaluated as previously discussed.[31] The resulting predictions for $R_e/R_e^{6:6}$, plotted in Figure 2, are seen, as predicted from the above analysis, to be closer to unity than those derived without considering dispersion. The differences are greater for the RbI and CsI because these species have the largest dispersive attractions.

4. Global Analysis of the Cohesive Energetics

The total binding energy $U(a,b)$ of each nanocrystal expressed as a ratio to that of the bulk is readily derivable from the present theory. This also enables one to calculate the energy gains in the different stages of relaxing the nanocrystal to its equilibrium geometry, all measured relative to the bulk lattice energy. These energy ratios can be converted into absolute values simply by invoking the experimental values for the bulk lattice energies. For CsI, only the lattice energy of its most stable phase, that having the 8-fold coordinated CsCl structure, is known experimentally. However, computations using the RIP predict that the lattice energy of the 6:6 phase is only 6 kJ/mol less than that (610 kJ/mol[18]) of the 8:8 structure, a prediction qualitatively similar to the experimental (5.6 kJ/mol[40,41]) difference between the energies of these two phases of CsCl. Hence, using the lattice energy for the 8:8 structure will only introduce errors of about 1% into the absolute energies to be presented for nanocrystalline CsI.

Equilibrium condition 14 applied to the bulk for which $2\ln 2 + M_b(1) = M_{6:6}$ and $C = 4$ yields

$$\frac{A}{(R_e^{6:6})^n} = \frac{M_{6:6}}{6nR_e^{6:6}} \qquad (66)$$

TABLE 8: Ratios Relative to the Bulk of the Energies of Nanocrystals, Unrelaxed $U(R_e^{6:6})/U_{6:6}(R_e^{6:6})$ and Relaxed $U(R_e)/U_{6:6}(R_e^{6:6})$, to the Constrained ($a = b$) Equilibrium Geometry

	$U(R_e^{6:6})/U_{6:6}(R_e^{6:6})$			$U(R_e)/U_{6:6}(R_e^{6:6})$		
crystallite	$n = 6$	$n = 10.5$	$n = 12$	$n = 6$	$n = 10.5$	$n = 12$
1 × 1	0.8853	0.8417	0.8351	0.9435	0.8691	0.8583
2 × 1	0.9321	0.8980	0.8928	0.9586	0.9106	0.9036
2 × 2	0.9593	0.9362	0.9327	0.9691	0.9409	0.9367
3 × 3	0.9748	0.9592	0.9569	0.9787	0.9611	0.9585
4 × 4	0.9838	0.9719	0.9701	0.9859	0.9729	0.9710

Substitution of this result into 12 evaluated for the bulk with $a = b = R_e^{6:6}$ yields the standard result for the bulk cohesive energy

$$U_{6:6}(R_e^{6:6}) = -\frac{M_{6:6}}{R_e^{6:6}}\left(1 - \frac{1}{n}\right) \qquad (67)$$

The cohesive energy $U(R_e^{6:6})$ of the nanocrystal evaluated at the equilibrium geometry of the bulk, a constrained structure with $a = b = R_e^{6:6}$, is found, from 12 after using 66 to eliminate A, to be given by

$$U(R_e^{6:6}) = -\frac{1}{R_e^{6:6}}\left(M_R - \frac{M_{6:6}(2 + C)}{6n}\right) \qquad (68)$$

Division of this result by eq 67 yields

$$\frac{U(R_e^{6:6})}{U_{6:6}(R_e^{6:6})} = \frac{\dfrac{M_R}{M_{6:6}} - \dfrac{2 + C}{6n}}{1 - \dfrac{1}{n}} \qquad (69)$$

This shows, in the hard sphere limit ($n \rightarrow \infty$), that the ratio of the binding energies is just that of the Madelung energies. These become more negative as the cross section of the nanocrystal increases toward the bulk value. This fractional loss of cohesive energy decreases with decreasing n because the number of short-range repulsions in the smaller nanocrystals is less than that from the six neighbors in the bulk. The quantitative results are presented in the first three numerical columns in Table 8.

The cohesive energy $U(R_e)$, at the relaxed but constrained ($x = 1$) optimum geometry of the nanocrystal, is given by an expression differing from 67 only in the replacement of $M_{6:6}$ by M_R and of $R_e^{6:6}$ by R_e. Division of this result by eq 67 followed by invoking 16 to eliminate the ratio of the equilibrium distances yields

$$\frac{U(R_e)}{U_{6:6}(R_e^{6:6})} = \frac{M_R}{M_{6:6}}\left(\frac{6}{2 + C}\frac{M_R}{M_{6:6}}\right)^{1/(n-1)} \qquad (70)$$

The numerical values of this ratio, presented in the three right most columns of Table 8, show, when compared with the corresponding values of $U(R_e^{6:6})/U_{6:6}(R_e^{6:6})$, that the energy gains on relaxation decrease both with increasing n and nanocrystal cross section. These relaxations occur because the reduction in the magnitude of the attractive Madelung terms on passing from the bulk to the nanocrystal is less than that of the short-range repulsions, reduced by virtue of the lower coordination number.

For any actual nanocrystal, a numerical value for the energy gained through relaxation (E_{relax}), equal to the difference

Model for Properties of Nanocrystalline Ionic Solids

J. Phys. Chem. B, Vol. 110, No. 12, 2006 **5947**

TABLE 9: Energies ($E_{relax} = U(R_e^{6:6}) - U(R_e)$) on Relaxing to the Constrained ($a = b$) Equilibrium Nanocrystal Geometries and Differences ($\Delta D_e = U(R_e) - U_{6:6}(R_e^{6:6})$) between the Bulk and Nanocrystal Lattice Energies (in kJ/mol)

	LiF ($D_e = 1036$)[19]		KI ($D_e = 649$)[19]		CsI ($D_e = 610$, see text)	
crystallite	E_{relax}	ΔD_e	E_{relax}	ΔD_e	E_{relax}	ΔD_e
1×1	60.3	58.5	17.8	85.0	14.2	86.4
2×1	27.5	42.9	8.2	58.0	6.6	58.8
2×2	10.2	32.0	3.0	38.4	2.4	38.6
3×3	4.0	22.1	1.2	25.2	1.0	25.3
4×4	2.2	14.6	0.7	17.6	0.6	17.7

TABLE 10: Ratios of $U(a_e, b_e)/U_{6:6}(R_e^{6:6})$ of Lattice Energies of the Fully Relaxed Nanocrystals Relative to the Bulk and Nanocrystal Energies Gained ($U(R_e) - U(a_e, b_e)$) on Relaxing the $a = b$ Constraint (in kJ/mol)

	$U(a_e, b_e)/U_{6:6}(R_e^{6:6})$			$U(R_e) - U(a_e, b_e)$		
crystallite	$n = 6$	$n = 10.5$	$n = 12$	$n = 6$	$n = 10.5$	$n = 12$
2×1	0.9613	0.9114	0.9042	2.8	0.52	0.37
2×2	0.9707	0.9414	0.9371	1.7	0.32	0.24

$U(R_e^{6:6}) - U(R_e)$, can be derived by subtracting the numerical value of 69 from that of 70 and then multiplying by the experimental lattice energy. Results for LiF, KI, and CsI, for which n takes the values of 6, 10.5, and 12, respectively, are presented in Table 9. Although these energy gains are appreciable for the smaller nanocrystals, particularly for LiF, they decrease rapidly with increase of both n and crystal size until becoming small for the 3×3 and 4×4 CsI systems. The difference (ΔD_e) between the total lattice energy of any nanocrystal and that of the bulk can be derived by subtracting from unity the ratio $U(R_e)/U_{6:6}(R_e^{6:6})$ and then multiplying by the experimental bulk lattice energy. The results, presented in Table 9, show that the greatest fractional energy losses arise for large values of n for which, as already shown, relaxation produces the least energy gain.

The removal of the constraint $x = 1$ relaxes the nanocrystal to its true minimum energy $U(a_e, b_e)$. The derivation of the ratio of this energy to that of the bulk is facilitated by defining the quantity y by

$$y = \frac{b_e}{R_e^{6:6}} \quad (71)$$

Cohesive energy expression 12 evaluated at the equilibrium geometry can be written in terms of this variable as

$$U(a_e, b_e) = -\frac{2 \ln 2 + M_b(x)}{y R_e^{6:6}} + (2 + Cx^{-n})\frac{A}{(y R_e^{6:6})^n} \quad (72)$$

After using 66 to eliminate A and then dividing the result by 67, one obtains

$$\frac{U(a_e, b_e)}{U_{6:6}(R_e^{6:6})} = \left(\frac{2 \ln 2 + M_b(x)}{y M_{6:6}} - \frac{2 + Cx^{-n}}{6ny^n}\right)\frac{1}{1 - \frac{1}{n}} \quad (73)$$

The numerical values of this ratio for 2×1 and 2×2 nanocrystals are presented in Table 10. An absolute value for the energy, $U(R_e) - U(a_e, b_e)$, gained on relaxation from the optimal constrained ($x = 1$) structure is derived by subtracting the value of $U(R_e)/U_{6:6}(R_e^{6:6})$ presented in Table 8 from the corresponding ratio $U(a_e, b_e)/U_{6:6}(R_e^{6:6})$ in Table 10 and then

TABLE 11: Comparison between Theoretical and Experimental Values of the Fractional Longitudinal Contractions $b_e/R_e^{6:6}$ and the Absolute Longitudinal Spacings b_e[a]

	$b_e/R_e^{6:6}$			b_e		
crystallite	$A = A_{6:6}$	$A = fA_{6:6}$	exp	$A = A_{6:6}$	$A = fA_{6:6}$	exp
KI (2×2)	0.957	0.964	0.979	6.389	6.436	6.538
KI (3×3)	0.973	0.977	0.984	6.496	6.522	6.566
RbI (3×3)	0.975	0.980	0.981	6.762	6.801	6.803
CsI (2×2)	0.963	0.971	0.969	6.943	6.999	6.992

[a] The theoretical b_e values are derived from $b_e/R_e^{6:6}$ multiplied by the experimental $R_e^{6:6}$. The values of f are derived from RIP computations, as described in the text.

multiplying by the experimental lattice energy. The results for LiF, KI, and CsI are presented in Table 10. The results show that these energy gains range from the small, for LiF, to the almost insignificant, for 2×2 crystals of both KI and CsI.

The ab initio quantum chemistry computations, described in the last section, for finite sized pieces of the 2×2 nanocrystal also provide evidence for the reliability of the predictions from the Born model. The results showed that the energy gain on making 1 mol of new contacts in a process of the type $m(LiF)_2 + p(LiF)_2 \rightarrow (m + p)(LiF)_2$ was essentially constant at 224 kJ/mol of planes being independent of m and p.[20] Here, the species $m(LiF)_2$ consists of m of the planes containing two cations and two anions. An independent computation[42] for the $m = p = 1$ case yielded the same result. A 1 mol portion of LiF stoichiometric formula units of the 2×2 nanocrystal can be constructed from its constituent gas-phase ions by first forming $N_A/2$ single $(LiF)_2$ planes and then assembling these planes, the latter process releasing 112 kJ/mol of formula units. Addition of the 887.2 kJ[42] computed for the heat of formation of these $N_A/2$ isolated planes predicts the lattice energy of the 2×2 nanocrystal to be 999 kJ/mol. This agrees well with the value of 1006 kJ/mol derived by combining the Born model lattice energy ratio presented in Table 9 with the experimental bulk value of 1036 kJ/mol.[19]

5. Discussion

The elucidation through microscopy of the structures of both 2×2 (ref 10) and 3×3 crystals[11] of KI as well as that of 3 $\times$ 3 RbI and 2×2 CsI crystals,[12] all encapsulated in singled walled carbon nanotubes of appropriate sizes, provided no evidence that the xy plane cross sections of any of these materials were not square. The separations b_e were measured to be 0.346, (0.695/2), 0.36, and 0.37 nm (or in atomic units: 6.538, 6.567, 6.803, and 6.992 au). These should be compared with spacings $R_e^{6:6}$ in bulk KI, RbI, and CsI of 6.676, 6.937 (ref 43), and 7.210 au (ref 44), respectively, at room temperature, that ambient in the experimental determination of the nanocrystal structures. The ratios $b_e/R_e^{6:6}$ derived from this experimental data are compared with the predictions of the present Born model in Table 11. The results in the second column were derived taking account of any difference between the A factors of the nanocrystal and those of the bulk using the approach described in section 3 based on the assumptions that the individual terms $V_s(R)$ and $E_{re}(R)$ are independent of structure with ,furthermore, their ratio being a constant f independent of interionic distance. The arguments of the type leading to result 54 then show that any differences between the A parameters in the nanocrystals and in the bulk will cause the $b_e/R_e^{6:6}$ predictions derived taking $A = A_{6:6}$ to be multiplied by the factor $(A/A_{6:6})^{1/(n-1)}$. The respective $A/A_{6:6}$ ratios of 15/14, 51/49, 1.0592, and 1.0928 for

the four encapsulated systems were derived from 53 using the values of unity, 1.1, and 1.1 for the f factors of KI, RbI, and CsI, these being reasonable averages of the RIP results for near equilibrium geometries. The resulting predictions for $b_e/R_e^{6:6}$ presented in column 2 were derived taking n to be 10.5, 11, and 12 for KI, RbI, and CsI, respectively. The predictions for b_e were derived as the product of the theoretical $b_e/R_e^{6:6}$ and the experimental bulk $R_e^{6:6}$. The theoretical predictions in Table 11 are entirely consistent with the experimental results in view of the ±0.02 nm (±0.38 au) precision[10−12] of the measured distances. Thus, there is no evidence that the observed contractions have any cause other than those of the interplay between the point Coulombic attractions and near neighbor short-range repulsions elucidated here for the free nanocrystals. The predictions derived taking account of the structural dependence of A do seem to be in slightly better agreement with the experiment than those derived taking $A = A_{6:6}$ although the experimental precision means that it cannot be stated that the latter are not also consistent with the experiment.

The prediction from Table 4 that the a_e/b_e ratios for all three systems are greater than unity, being 1.024, 1.012, 1.011, and 1.010, respectively, is consistent with the values of 1.156, 1.065, 1.083, and 1.108 derived from the experimentally measured[10−12] a_e values of 0.4, 0.37, 0.39, and 0.41 nm (or in atomic units: 7.559, 6.992, 7.370, and 7.748 au). This shows that the observation of the gross results that the a_e/b_e ratios are greater than one is a property of the nanocrystal itself and is explicable from the present theory and that ratios greater than one are not therefore caused by interaction with the wall. However, the result that the a_e/b_e ratios predicted for the free nanotube are significantly less than the experimental values, even though all ratios are greater than one, strongly suggests that interactions with the nanotube walls are significant. This conclusion agrees with the finding of a previous study[15,16] of the encapsulated KI system, which used empirical potentials, that the computed a_e/b_e ratios were greater than unity but less than experimental values without considering interactions with the wall. It should be noted that the computed a_e/b_e ratio only agreed quantitatively with experimental value if the nanotube was considered to be surrounded by molten salt. However, there was no such molten salt surrounding the nanotubes during the measurements of their structures. The importance of ion−wall interactions in the determination of a_e is reinforced by the predictions, derived from the results in Table 4, that $a_e/R_e^{6:6}$ is 0.978, 0.985, 0.992, and 0.982 for the three encapsulated crystals. These values, being less than unity, are not consistent with the experiment because each of the latter a values is greater than the corresponding bulk separation $R_e^{6:6}$. Furthermore, even after introducing the factor of $(A/A_{6:6})^{1/(n-1)}$ arising on considering the structural dependence of A, the ratios of 0.982, 0.989, 0.998, and 0.990 predicted for a_e/b_e remain less than unity.

6. Conclusions

This paper has presented a theory of the structure, energetics, and relationships between nanocrystals generated as small sections of ionic crystals having the rock-salt structure. These nanocrystals consist of m_1 rows and m_2 columns of ions of alternating charges, the columns being infinite in extent along the ⟨001⟩ z direction. The theory, based on the assumption that these crystals are fully ionic, focuses only on the largest and most important terms, namely, the Coulombic interactions between the ions treated as point charges and the short-range repulsive interactions between just immediately neighboring ions. The latter interactions were described in the original Born

form Ar^{-n}. The structures of such nanocrystals are defined by the distances a and b between closest ions respectively perpendicular and parallel to the z direction.

The shapes of the nanocrystals, defined by the ratio a_e/b_e, were shown to be independent of the strength A of the short-range repulsion. Furthermore, their sizes relative to the bulk, as defined by the ratio $b_e/R_e^{6:6}$ were also found to independent of A if this was taken to independent of structure. Hence, the only property of this repulsion which governs any of these ratios is the range n of the repulsion, this decreasing with increase of n. This shows that the chemical dependence of the structures is determined solely by n. Both the ratios $b_e/R_e^{6:6}$ and $a_e/R_e^{6:6}$ were shown to be less than unity with a_e/b_e being larger than one. All these ratios were shown to become closer to unity on increase of either n or the crystal cross section as defined by the numbers of rows and columns. Thus, the structure reduces to that of the bulk either as n tends to infinity or as both m_1 and m_2 tend to infinity, the former corresponding to the limit in which the ions behave as hard spheres. The result that the Madelung binding within a single chain is much greater than that between different chains, even for those immediately adjacent, explains why b_e is less than a_e even for the systems of a 2×1 cross section in which each ion experiences two intrachain short-range repulsions but only a single interchain short-range repulsion.

The Born repulsion is actually an effective repulsion composed of contributions from the true short-range repulsion $V_s(b)$ and the rearrangement energy required to convert a free anion into its form optimal for a crystal with the specified geometry. The A parameter was shown to increase with decreasing nanocrystal cross section if the two components of the effective repulsion were structurally independent. Although the predicted ratios $b_e/R_e^{6:6}$ and $a_e/R_e^{6:6}$ were shown to be increased on considering such structural dependence of A, the prediction that these ratios are less than one remained unchanged. The a_e/b_e ratio remains unaffected by any variation of A between the bulk and the nanocrystal because this ratio is a property solely of the latter. For the single chain system, it was possible to introduce explicitly the interionic dispersive attractions rather than allowing these to be considered only implicitly, as in the Born model, through the introduction of both experimental interionic separations and the use of n values determined from experimental compressibility measurements. It was shown that such explicit introduction of the dispersive attractions increased the predicted ratio of $b_e/R_e^{6:6}$ although this still remained significantly less than unity.

It was shown that it is useful to consider relaxing the nanocrystal to its equilibrium structure in two stages from an initial configuration in which the interionic separations equal those of the bulk. In the first of these, the nanocrystal is relaxed under the constraint that $a = b = R_e$, this constraint being removed in the second stage. The ratio $R_e/R_e^{6:6}$ was shown to be less than one and to increase toward unity as either n or the nanocrystal cross section is increased. This ratio decreases with reduction of the nanocrystal cross section because, for fixed R, the number of short-range repulsions decreases more rapidly than does the magnitude of the attractive Madelung term. The energy gained in each of these two stages decreases with increase of crystal cross section and n, there being no energy gain in the hard sphere limit of infinite n. The energy gained in the first stage is very much greater than that in the second stage, even the largest value for the latter being only some 3 kJ/mol for a 2×1 LiF nanocrystal. For the 2×2 and 3×3 KI systems, these energy gains of 0.5 and 0.3 kJ/mol, respectively, are still

Model for Properties of Nanocrystalline Ionic Solids

J. Phys. Chem. B, Vol. 110, No. 12, 2006 **5949**

less than those of 3.0 and 1.2 kJ/mol in the first stage. Although even the latter energy gains are quite modest, they become more significant for the smaller crystals with low n.

The first of four principle insights revealed by the present work is that the experimentally determined values for b_e are entirely consistent both qualitatively and quantitatively with the predictions of the present theory. There is therefore no evidence that the encapsulating nanocrystal plays any role in determining this parameter which has therefore been shown to emerge from the interplay between just the two largest interactions within the nanocrystal. However, although the present theory correctly predicts that a_e is greater than b_e, the measured ratios of a_e/b_e are significantly greater than the present predictions and, furthermore, the measured distances a_e are greater than the $R_e^{6:6}$ values of the bulk in contradiction to the prediction that $a_e/R_e^{6:6}$ is less than one. This suggests very strongly that interaction with the nanotube wall plays a significant role in determining this parameter, a topic to be addressed elsewhere.

The second main physical insight from the present work is that the molar binding within a single chain of infinite length is significantly greater than that between the chains, thereby explaining why the ratio of a_e/b_e is greater than unity even in the absence of any encapsulation. This renders fully transparent the third conclusion that the distance b_e is contracted relative to the bulk as a consequence of the greater intrachain binding, the fractional reduction of the Madelung energy on passing from the bulk to a nanocrystal being much less than that of the short-range cation−anion repulsion. The fourth insight revealed by the present work is that the ratios a_e/b_e depend only on the range of the short-range repulsion as defined by the Born exponent n and not on the strength as manifested by the A parameter.

References and Notes

(1) Sloan, J.; Hammer, J.; Zwiefka-Sibley, M.; Green, M. L. H. *Chem. Commun.* **1998**, *3*, 347−348.

(2) Kiang, C. H.; Choi, J. S.; Tran, T. T.; Bacher, A. D. *J. Phys. Chem. B* **1999**, *103*, 7449−7451.

(3) Sloan, J.; Wright, D. M.; Bailey, S. R.; Brown, G.; York, A. P. E.; Coleman, K. S.; Green, M. L. H.; Hutchison J. L.; Woo, H. G. *Chem. Commun.* **1999**, *8*, 699−700.

(4) Govindaraj, A.; Satishkumar, B. C.; Nath, M.; Tao, C. N. R. *Chem. Mater.* **2000**, *12*, 202−205.

(5) Hirahara, K.; Suenaga, K.; Bandow, S.; Kato, H.; Okazaki, T.; Shinohara, H.; Iijima, S. *Phys. Rev. Lett.* **2000**, *85*, 5384−5387.

(6) Suenaga, K.; Tencé, M.; Mory, C.; Colliex, C.; Kato, H.; Okazaki, T.; Shinohara, H.; Hirahara, K.; Bandow, S.; Iijima, S. *Science* **2000**, *290*, 2280−2282.

(7) Mittal, J.; Monthioux, M.; Allouche, H.; Stephan, O. *Chem. Phys. Lett.* **2001**, *339*, 311−318.

(8) Xu, C.; Sloan, J.; Brown, G.; Bailey, S. R.; Clifford Williams, V.; Friedrichs, S.; Coleman, K. S.; Flahaut, E.; Green, M. L. H.; Hutchison J. L.; Dunin-Borkowski, R. E. *Chem. Commun.* **2000**, *24*, 2427−2428.

(9) Meyer R. R.; Sloan, J.; Dunin-Borkowski, R. E.; Kirkland, A. I.; Novotny M. C.; Bailey, S. R.; Hutchison, J. L.; Green, M. L. H. *Science* **2000**, *289*, 1324−1326.

(10) Sloan, J.; Novotny, M. C.; Bailey, S. R.; Brown, G.; Xu, C.; Williams, V. C.; Friedrichs, S.; Flahaut, E.; Callender, R. L.; York, A. P. E.; Coleman, K. S.; Green, M. L. H.; Dunin-Borkowski, R. E.; Hutchison, J. L. *Chem. Phys. Lett.* **2000**, *329*, 61−65.

(11) Sloan, J.; Friedrichs, S.; Meyer, R. R.; Kirkland, A. I.; Hutchison, J. L.; Green, M. L. H. *Inorg. Chem. Acta* **2002**, *330*, 1−12.

(12) Sloan, J.; Kirkland, A. I.; Hutchison, J. L.; Green, M. L. H. *Compt. Rend. Phys.* **2003**, *4*, 1063−1074.

(13) Brown, G.; Bailey, S. R.; Sloan, J.; Xu, C.; Friedrichs, S.; Flahaut, E.; Coleman, K. S.; Green, M. L. H.; Dunin-Borkowski, R. E. *Chem. Commun.* **2001**, *9*, 845−846.

(14) Sloan, J.; Kirkland, A. I.; Hutchison, J. L.; Green, M. L. H. *Chem. Commun.* **2002**, *13*, 1319−1332.

(15) Wilson, M.; Madden, P. A. *J. Am. Chem. Soc.* **2001**, *123*, 2101−2102.

(16) Wilson, M. *J. Chem. Phys.* **2002**, *116*, 3027−3041.

(17) Wilson, M. *Chem. Phys. Lett.* **2002**, *366*, 504−509.

(18) Johnson, D. A. *Some thermodynamic aspects of inorganic chemistry*; Cambridge University Press: Cambridge, 1968.

(19) Weast, R. C. *CRC Handbook of chemistry and physics*, 59th ed.; CRC Press: Boca Raton, FL, 1979.

(20) Bichoutskaia, E.; Pyper, N. C. *Chem. Phys. Lett.* **2005**, submitted for publication.

(21) Nada, R.; Catlow, C. R. A.; Pisani, C.; Orlando, R. *Modell. Simul. Mater. Sci. Eng.* **1993**, *1*, 165−187.

(22) Löwdin, P. O. *J. Chem. Phys.* **1950**, *18*, 365−375.

(23) Gale, J. D.; Rohl, A. L. *Mol. Simul.* **2003**, *29*, 291−341.

(24) Wood, C. P.; Pyper, N. C. *Chem. Phys. Lett.* **1981**, *81*, 395−401.

(25) Wood, C. P.; Pyper, N. C. *Philos. Trans. R. Soc. London, Ser. A* **1986**, *320*, 71−105.

(26) Pyper, N. C. *Philos. Trans. R. Soc. London, Ser. A* **1995**, *352*, 89−124.

(27) Harding, J. H.; Lindan, P. J. D.; Pyper, N. C. *J. Phys.: Condens. Matter* **1994**, *6*, 6485−6496.

(28) Pyper, N. C. *J. Phys.: Condens. Matter* **1995**, *7*, 9127−9145.

(29) Pyper, N. C. *J. Phys.: Condens. Matter* **1996**, *8*, 5509−5525.

(30) Pyper, N. C. *Chem. Phys. Lett.* **1994**, *220*, 70−76.

(31) Pyper, N. C. *J. Chem. Phys.* **2003**, *118*, 2308−2324.

(32) Pyper, N. C. *Adv. Solid State Chem.* **1991**, *2*, 223−393.

(33) Pyper, N. C. *Philos. Trans. R. Soc. London, Ser. A* **1986**, *320*, 107−158.

(34) Madden, P. A.; Wilson, M. *Chem. Soc. Rev.* **1996**, *25*, 339−350.

(35) Mahan, G. D. *Solid State Ionics* **1980**, *1*, 29−45.

(36) Fowler, P. W.; Madden, P. A. *Mol. Phys.* **1983**, *49*, 913−923.

(37) Fowler, P. W.; Madden, P. A. *Phys. Rev. B* **1984**, *29*, 1035−1042.

(38) Jacobi, N.; Csanak, Gy. *Chem. Phys. Lett.* **1975**, *30*, 367−372.

(39) Lennard-Jones, J. E.; Ingham, J. E. *Proc. R. Soc. London, Ser. A* **1925**, *107*, 636−653.

(40) Zemczunzy, S.; Rambach, F. *Z. Anorg. Chem.* **1910**, *65*, 403−428.

(41) Wagner, G.; Lippert, L. *Z. Phys. Chem.* **1936**, *B31*, 263−274.

(42) Lintuluoto, M. *J. Mol. Struct. (THEOCHEM)* **2001**, *540*, 177−192.

(43) Landolt-Bornstein, Z., series III; Springer: Berlin, 1966; Vol. 1.

(44) Blackman, M.; Khan, I. H. *Proc. Phys. Soc., London* **1961**, *77*, 471−475.